A Compressive-Sensing-Based Approach for the Detection and Characterization of Buried Objects

Michele Ambrosanio, *Student Member, IEEE*, and Vito Pascazio, *Senior Member, IEEE*

***Abstract*—The problem of determining and understanding the nature of buried objects by means of nondestructive and noninvasive techniques represents an interesting issue for a great variety of applications. In this framework, the theory of electromagnetic inverse scattering problems can help in such an issue by starting from the measures of the scattered field collected on a surface. What will be presented in this communication is a two-dimensional (2-D) technique based on the so-called Born approximation (BA) combined with a compressive sensing (CS) approach, in order to improve reconstruction capabilities for a proper class of targets. The use of a multiview-multistatic configuration will be employed together with a multifrequency approach to overcome the limited amount of data due to the single-frequency technique. Therefore, after a first numerical analysis of the performance of the considered algorithm, some numerical examples for 2-D aspect-limited configurations will be presented. The scenario is composed of a simplified scene, which consists of two half-spaces, and with the probes located close to the interface between the two media. As proposed in the following, it is easy to observe that the use of CS for this kind of problems may improve reconstruction capabilities, confirming the validity of the presented approach.**

***Index Terms*—Compressive sensing (CS), electromagnetic inverse scattering, ground penetrating radar, microwave tomography.**

I. Introduction

THE CAPABILITY of electromagnetic fields to penetrate different materials makes them very attractive to reconstruct, both in a qualitative and quantitative way, the morphological and electrical features of the unknown objects by means of a ondestructive technique, which starts from the measures of the scattered field. Such a technique may be applied in several field, including geophysics [1], characterization of materials [2], monitoring in biomedical engineering [3], and demining applications [4].

In the framework of the so-called aspect-limited problems, an interesting application is related to ground penetrating radar (GPR), which employs signals whose frequencies vary from a few hundreds of megahertz till to some gigahertz according to the considered scenario. As most of the techniques based on radar approaches, target information is retrieved from the two-travel time of a pulse radiated by a source and gathered by a fixed-offset system between transmitter and receiver [5]. The image obtained by joining the radar echoes collected while moving the antennas is referred to as a raw data "radargram."

Unfortunately, what radar techniques usually allow is only the extraction of qualitative information on the investigated region that is based on a subjective interpretation of the raw data and on user experience. Therefore, since in many cases, it is not possible to provide detailed information on the targets, several data processing techniques have been proposed, among which one can find focalization procedures [6] and tomographic techniques [7].

Among all these techniques, tomographic imaging seems to be a promising approach to overcome the limitations related to standard procedures, since it makes possible to achieve not only information about the shape and localization of buried objects, but it also allows a quantitative electromagnetic characterization of these targets in the imaging domain under test [8].

Nevertheless, the detection performance of GPR largely depends on a lot of factors, which can partially or totally hide or distort the response of the buried targets. Among all these factors, it is remarkable to cite the coupling between antennas and soil, the electromagnetic features of the background, the speed and scattering of wave propagation, and the electromagnetic contrast of the buried objects on which the intensity of the scattered fields depends [9].

Therefore, there is a need to develop appropriate techniques for clutter reduction and subsurface imaging. In this category, detection techniques are employed on a subsurface image built from a full GPR scan after clutter reduction. They include advanced algorithms for hyperbola detection [10]–[13], and migration approaches [14], [15]; their performance mainly depends on the data set quality and on the preprocessing method used to subtract the contribution of the background.

In this framework, a great variety of tomographic techniques may be found in the literature to find a solution to the electromagnetic inverse scattering problem previously described [16]–[20]. More in detail, it is possible to divide these approaches in two main classes: the first one faces the inverse scattering problem without any approximation and, in principle, this class can provide an accurate reconstruction of the region under test, but it drives into a nonlinear ill-posed inverse problem, and

Manuscript received September 30, 2014; revised February 03, 2015; accepted March 23, 2015. Date of publication June 11, 2015; date of current version August 11, 2015. The work was supported in part by FP7 D-BOX Project under Grant 284996 and in part by an European Consortium within the European Commission Seventh Framework Programme (FP7).

The authors are with the Dipartimento di Ingegneria, University of Napoli Parthenope, Centro Direzionale di Napoli, Isola C4, 80143 Napoli, Italy, and also with Consorzio Nazionale Interuniversitario per le Telecomunicazioni (CNIT), Unità di Napoli Parthenope, 80143 Napoli, Italy (e-mail: michele.ambrosanio@uniparthenope.it; vito.pascazio@uniparthenope.it).

Color versions of one or more of the figures in this paper are available online at http://ieeexplore.ieee.org.

Digital Object Identifier 10.1109/JSTARS.2015.2421812

a second class of approximated approaches which simplifies the model. Even though the first class of algorithms may realize better quantitative reconstructions, the nonlinearity of the model makes the solution of such problems be usually very sensitive to the availability of adequate information about the reference scenario, so that any sensible information about the scene has to be dealt with: such a feature may limit their applicability since an accurate knowledge of the electromagnetic features of the scenario is required to model correctly the problem. Despite the increasing interest in this class of approaches, the inaccuracy in the knowledge of the reference scenario (soil permittivity and conductivity) and the not-perfect knowledge of the antennas radiation characteristics in the presence of the soil affect the quality of the reconstruction problems. Moreover, the nonlinearity of the relationship between data and unknowns may drive into false solutions that still exist, thus affecting the reliability of the overall solution strategy [21], [22], and increasing the computational time. The second class of solution approaches exploits simplified models of the electromagnetic scattering to develop linear inversion approaches [23]–[25].

What has been proposed in this paper is an inversion strategy which belongs to the second class of the approaches presented before, since it is based on the so-called Born approximation (BA). Due to the linearity of the problem, the solution is searched as the global minimum of a quadratic cost function, for which no false-solutions exist. Moreover, for linear inverse problems, the adoption of well-assessed regularization schemes [26] is possible and reconstruction capabilities can be foreseen.

Despite of the advantages said above by the adoption of such models, the class of targets that may be recovered is limited to those objects for which the BA is still valid, as for small objects whose electromagnetic features are very close to those of the background. In addition, since the aspect-limited nature of data implies that single-frequency data are not sufficient to realize effective inversions, a multifrequency approach will be considered throughout this communication. In order to assess the actual performance of the approach in a relatively simple situation, the canonical and significant two-dimensional (2-D) geometry is considered, together with the use of a regularization technique based on compressive sensing (CS), which makes it possible to reduce the number of data considerably.

This paper is organized as follows. In Section II, the statement of the problem and some basic knowledge about the employed multifrequency approach are presented by starting from the general nonlinear model of the electromagnetic scattering phenomenon. Then, in Section III, a simplified, linearized model, and a standard inversion procedure is proposed. In order to overcome some restrictions, the theory of CS is quickly described in Section IV and a preliminary analysis of the performance of such an approach has been proposed for the ideal case of homogeneous medium in Section V, in which CS has been used as a regularization strategy. Finally, some numerical results for the GPR applications are shown in Section VI. Conclusion follows in Section VII.

II. Problem Statement

The reference geometry is represented by the scalar 2-D scenario depicted in Fig. 1. In this framework, a homogeneous half-space rather than a multilayered background has been assumed. The homogeneous medium surrounding the objects is characterized by a complex permittivity ϵ_2 and all the targets inside the imaging domain, including the background medium, have a magnetic permeability that is everywhere equal to μ_0. All the targets are located in the lower half-space, whereas the sources of the electromagnetic field are located in the upper medium. Such sources are filamentary z-directed electric current (TM polarization) in which the current is constant and put along a line close to the interface which separates the two media. Assuming that also scatterers features are invariant along the z-direction, the data are collected by moving the sources into N_v different positions along the observation line Γ and, for each illumination, N_m measures at the receiving probes are picked up along the same line. Therefore, the measurement configuration works in reflection mode and the set-up is a multiview-multistatic one, in which the scattered field is measured in several locations along Γ for each position of the source. The goal of this analysis is to determine the unknown contrast function χ inside the imaging domain Ω, defined as

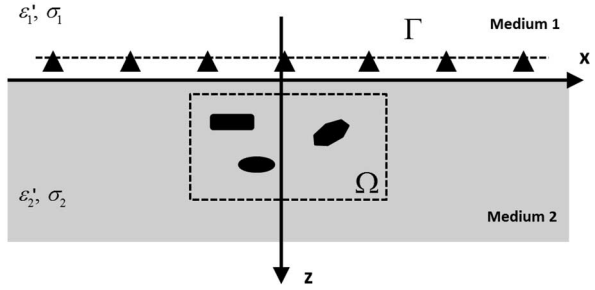

Fig. 1. Reference geometry. Γ represents the measuring line on which all the probes (transmitters and receivers) are located (medium 1), whereas Ω is the imaging domain buried in the soil (medium 2).

$$\chi(\boldsymbol{r},\omega) = \frac{\epsilon_x(\boldsymbol{r},\omega)}{\epsilon_2(\omega)} - 1 \tag{1}$$

where $\epsilon_x(\boldsymbol{r},\omega) = \epsilon_x'(\boldsymbol{r}) - j\frac{\sigma_x(\boldsymbol{r})}{\omega\epsilon_0}$ and $\epsilon_2(\omega) = \epsilon_2' - j\frac{\sigma_2}{\omega\epsilon_0}$ are the complex permittivities of the unknown targets and background, respectively.

In this framework, due to the aspect limited geometry of the considered scenario, the electromagnetic scattering problem can be recast in the following integral relationships [27], [28]:

$$\begin{aligned} E_{tot}^{(v)}(\boldsymbol{r},\omega) &= E_{inc}^{(v)}(\boldsymbol{r},\omega) \\ &\quad + k_2^2 \int_\Omega g_{22}(\boldsymbol{r},\boldsymbol{r'},\omega)\chi(\boldsymbol{r'},\omega)E_{tot}^{(v)}(\boldsymbol{r'},\omega)d\boldsymbol{r'} \\ &= E_{inc}^{(v)}(\boldsymbol{r},\omega) + A_i[\chi E_{tot}^{(v)}], \quad \boldsymbol{r}\in\Omega,\ v{=}1,\ldots,N_v \end{aligned} \tag{2}$$

$$\begin{aligned} E_{scat}^{(v)}(\boldsymbol{r},\omega) &= k_2^2 \int_\Omega g_{21}(\boldsymbol{r},\boldsymbol{r'},\omega)\chi(\boldsymbol{r'},\omega)E_{tot}^{(v)}(\boldsymbol{r'},\omega)d\boldsymbol{r'} \\ &= A_e[\chi E_{tot}^{(v)}](\boldsymbol{r},\omega), \quad \boldsymbol{r}\in\Gamma,\ v=1,\ldots,N_v \end{aligned} \tag{3}$$

in which the time exponential factor $e^{j\omega t}$ has been omitted. In the previous equations, $E_{inc}^{(v)}$ and $E_{tot}^{(v)}$ represent the incident and total fields for each position of the transmitting antennas

inside the imaging domain Ω, and $E_{scat}^{(v)}$ is the scattered field in the upper medium, whose samples are located on Γ. The parameter $k_2 = \omega\sqrt{\epsilon_2\epsilon_0\mu_0}$ is the complex wavenumber in the lower medium, while g_{2i}, with $i = 1, 2$, are the Sommerfeld–Green's functions of the considered geometry, which represent the field generated by a filamentary source located in medium 2 and observed in the medium "*i*." It is interesting to note that such functions represent the kernel of the integral operators in (2) and (3), and they are known as the internal and external electromagnetic scattering operators. It is worth to note that both these operators can be evaluated in a fast and efficient way by means of Fast Fourier Transform (FFT) codes, both for 2-D and three-dimensional (3-D) cases. These bilinear operators are defined as $A_i : X \times T \to S_i$ and $A_e : X \times T \to S_e$, with $X \subset L^{\infty}(\Omega)$ the subspace of the possible contrast functions, $T \subset L^2(\Omega)$ a proper subspace for the total electric field inside the object, and $S_i \subset L^2(\Omega)$ and $S_e \subset L^2(\Gamma)$ two proper subspaces for the scattered field inside and outside the imaging domain.

In order to recover the geometrical and electromagnetic features of the unknown targets in the lower medium in a quantitative way, one has to solve the system of (2) and (3) and determine the contrast function χ. Unfortunately, the formal inversion of such a system of equations is not easy, due to the nonlinear relationship between data and unknowns. Moreover, it is well known that such a problem is also ill-posed in the sense of Hadamard, both in the single-view and multiview cases. Therefore, false solutions may occur easily [29], [30], and in order to restore the well-posedeness, a regularization procedure is required. It is important to note that the ill-posedness of the problem is due to the finite dimensionality of the scattered field, as extensively discussed in [21].

The nonlinear equations (2) and (3) relating data and unknowns may be recast in [16]

$$E_{scat}^{(v)} = A_e\left[(I - \chi A_i)^{-1} \cdot \chi E_{inc}^{(v)}\right], \quad v = 1, \ldots, N_v \quad (4)$$

which has been achieved by substituting the domain equation (2) into the data equation (3) ("I" is the identity operator). Equation (4) clearly shows the nonlinearity of the relation between data E_{scat} and unknowns χ; such a nonlinear mapping can be linearized [31], exploiting the well-known BA, which amounts to assume the total field inside the imaging domain Ω equal to the incident field. Therefore, using the previous approximation, (4) becomes

$$E_{scat}^{(v)} = A_e\left[\chi E_{inc}^{(v)}\right] = L^{(v)}[\chi], \quad v = 1, \ldots, N_v. \quad (5)$$

The operator "$L^{(v)}$," incorporating $E_{inc}^{(v)}$ in A_e, is a linear mapping between data $E_{scat}^{(v)}$ and unknown χ. It has to be pointed out that the linearization of model (4) into (5) does not overcome the ill-posedness of such an inverse problem, due to the finite-dimensional nature of the scattered field. The order of the finite-dimensional nature reduces further when accounting the aspect-limited nature of the considered problem. The more critical the aspect-limited is, the lower the order of the finite dimension and the more critical the capability to recover profiles is. Hence, in order to improve the reconstruction performances of the tomographic approach, one may collect more information using multifrequency data, since monochromatic data may be too poor to guarantee good results, as shown in the spectral coverage of the multiview-multistatic multifrequency configuration shown in the following (see Section VI).

In choosing a multifrequency approach, some attention has to be paid in defining the unknown of the problem, since the contrast function, which represents the unknown of our problem, does not change with the illumination, but it changes with frequency. Nevertheless, the fact that the contrast function changes with the frequency would imply to solve more monochromatic inverse scattering problems, but since the dependence on the frequency in the complex permittivity of the media and buried objects is supposed to be as

$$\epsilon(\boldsymbol{r}, \omega) = \epsilon'(\boldsymbol{r}) - j\frac{\sigma(\boldsymbol{r})}{\omega\epsilon_0} \quad (6)$$

where $\epsilon'(\boldsymbol{r})$ and $\sigma(\boldsymbol{r})$ represent the permittivity and conductivity of the second medium and buried targets, with the hypothesis that they are independent from the frequency. Keeping in mind what has been said previously, it is possible to exploit the multifrequency data to improve the amount of independent information to gain better reconstructions. By means of simple changes in the expression of the contrast function, one can recover the unknown profile at a certain frequency (e.g., the maximum one) using all the bandwidth information. In this framework, the unknown contrast function can be written as [22]

$$\chi(\boldsymbol{r}, \omega) = \frac{1}{2}\left(1 + \frac{\overline{\omega}}{\omega}\right)\overline{\chi}(\boldsymbol{r}) + \frac{1}{2}\left(1 - \frac{\overline{\omega}}{\omega}\right)\overline{\chi}^{*}(\boldsymbol{r}) = B_{\omega}[\overline{\chi}] \quad (7)$$

where $\overline{\chi}(\boldsymbol{r}) = \chi(\boldsymbol{r}, \overline{\omega})$ is the value of the contrast function at the selected frequency, the mathematical symbol "$*$" represents the conjugate operation, and $B_{\omega}[\cdot]$ is a linear operator. Therefore, by looking at (7), by knowing the contrast function at the frequency $\overline{\omega}$, it is possible to evaluate the contrast function at any frequency in the chosen bandwidth. According to this approach, it is possible to benefit to have more data (multifrequency) at expenses of increasing of both measurements and computational burden, but leaving unchanged the same number of unknowns of the single-frequency case. As we will see in the following sections, in order to mitigate the burden, we will try to use as few as possible the number of frequencies in the widest allowable frequency bandwidth. Therefore, it is convenient to use a multifrequency approach rather than a monochromatic one, even though this leads to an increase of both measurements and computational burden, and this is the reason for collecting the data at a few frequencies in the widest allowable frequency bandwidth.

III. Linearized Scattering Model

According to the previous section, let us consider N_f working frequencies spanning a total bandwidth $(\omega_{max} - \omega_1)$ and let us assume as reference the maximum frequency

in the selected bandwidth, that means to assume that $\chi(\omega_{max}) = \chi(\omega_{N_f}) = \chi(\overline{\omega}) = \overline{\chi}$. Then, starting from (5), for the single-frequency case and moving toward a multifrequency approach, it is possible to write the system (8) shown at the bottom of the page which can be recast in a compact form that generalizes (5) to the multifrequency case for all the views

$$E_{scat}^{MF}(\boldsymbol{r}) = A_e^{MF}\left[B_\omega\left[\overline{\chi}(\boldsymbol{r})\right] \cdot E_{inc}^{MF}(\boldsymbol{r})\right] = L^{MF}\left[\overline{\chi}\right]. \quad (9)$$

The considered problem is still ill-posed and needs a regularization technique to achieve a reliable solution. Moreover, in order to tackle the ill-posedness, due to the finite amount of data, one has to look for a finite dimensional representation of the unknown profile. More in details, the contrast function χ may be represented as a finite-dimensional version $\hat{\chi}$ on the grid defining the discrete version of the imaging domain Ω. Although the contrast function should be referred to use the hat accent in a rigorous fashion, here we will omit such a symbol to simplify the notation. With these assumptions, we can express the contrast function as

$$\overline{\chi}(\boldsymbol{r}) = \sum_{p=1}^{P} c_p \phi_p(\boldsymbol{r}) \quad (10)$$

where $\{\phi_p\}_{p=1}^{P}$ is a suitable set of basis functions and the c_p is the coefficient of the unknown contrast. In a continuous space, the truncation index "P" should be infinite, but since we are dealing with a discrete version of the contrast function, in case of lack of any *a priori* information and additional forms of regularization, this number has to be lower than the essential dimension of data (i.e., the degrees of freedom) and can be determined by means of an analytic or numeric criterion (as it will be shown very quickly in the following).

In this paper, due to the aim of such a preliminary analysis and to the targets features, a pixel-fashioned basis will be adopted in order to define the scatterers in the imaging domain since such a basis fits well with the proposed CS-based approach, whose details will be presented in the following section. After the discretization of (9) on a certain grid [21] and introducing the multifrequency multiview-multistatic tomographic operator $\mathbf{L}^{MF}$: $L^2(\Omega) \to L^2(\Gamma)$, the mathematical model in presence of additive noise drives in

$$\mathbf{e}_{scat}^{MF} = \mathbf{L}^{MF}\overline{\boldsymbol{\chi}}_{2N_{cells}} + \mathbf{w} \quad (11)$$

where $\mathbf{e}_{scat}^{MF}$ and $\mathbf{w}$ are the vectors collecting all the samples of the scattered field (multifrequency and for all views) and noise, respectively, $\mathbf{L}^{MF}$ is the matrix which defines the linear model employed and $\overline{\boldsymbol{\chi}}_{2N_{cells}} = [\overline{\boldsymbol{\chi}}_{Re}; \overline{\boldsymbol{\chi}}_{Im}]$ is the vector of size $2N_{cells} \times 1$ which includes real and imaginary parts of contrast profile at reference frequency. More in detail, the generic element of the matrix $\mathbf{L}^{MF}$ is

$$\begin{aligned}
&l_{hn} = l_{mn}^{v}(\omega_f) = E_{inc}^{(v)}(\boldsymbol{r}_n, \omega_f) \iint_{\Omega(\boldsymbol{r}_n)} g_{21}(\boldsymbol{r}_m, \boldsymbol{r'}, \omega_f)\, d\boldsymbol{r'} \\
&\boldsymbol{r}_m \in \Gamma, \quad \boldsymbol{r}_n \in \Omega, \quad n = 1, \ldots, N_{cells} \\
&l_{hn} = l_{mn}^{v}(\omega_f) = j \cdot \alpha \cdot E_{inc}^{(v)}(\boldsymbol{r}_{n-N_{cells}}, \omega_f) \\
&\qquad \cdot \iint_{\Omega(\boldsymbol{r}_{n-N_{cells}})} g_{21}(\boldsymbol{r}_m, \boldsymbol{r'}, \omega_f)\, d\boldsymbol{r'}, \quad \boldsymbol{r}_m \in \Gamma \\
&\boldsymbol{r}_{n-N_{cells}} \in \Omega,\ n = N_{cells}+1, \ldots, 2N_{cells}
\end{aligned} \quad (12)$$

where $h = 1, \ldots, (N_m \times N_v \times N_f)$, $m = 1, \ldots, N_m$, $f = 1, \ldots, N_f$ and $v = 1, \ldots, N_v$, with N_{cells} equal to the number of cells in the grid of Ω and N_f equal to the number of frequencies employed (see Appendix for more details). Note that, for $n = 1, \ldots, N_{cells}$, $\Omega(\boldsymbol{r}_n)$ represents the nth cell of the considered imaging domain.

Since what we are going to propose is a preliminary analysis of a GPR technique for demining applications and due to the fact that mines in the soil are small enough compared with the wavelength at the operating frequencies, such targets can be described by using a few pixels in the discretized grid of a rect-function basis: this makes it possible to assume the sparseness of the targets and use the theory of CS.

IV. CS Theory: Basics

CS theory represents a good strategy for solving linear inverse scattering problems under some assumptions. It is based on the observation that many types of signals have a sparse expansion in terms of a suitable basis or frame; therefore, there is only a small number of expansion coefficients that are significant (i.e., nonvanishing entries). Therefore, such a technique is able to recover the unknown signal from very undersampled measurements. More in detail, CS relies on two principles: sparsity, which pertains to the signal of interest; and incoherence, which represents a classical way of analyzing the recovery capabilities of a measurement matrix.

A classical approach to solve linear problem is represented by the least squares (LS) approach, in which the estimator is chosen to minimize a proper functional. When the number of data is equal to the number of unknowns and the matrix that describes the model is nonsingular, the considered problem can be solved properly by inverting such a matrix; unfortunately inverse problem can be ill-posed, and thus the LS solution could not work properly. In order to overcome this difficulty, regularization methods are required to make the solution more

$$\begin{cases}
E_{scat}^{(v)}(\boldsymbol{r}, \omega_1) = A_{e_{\omega_1}}\left[\chi(\boldsymbol{r}, \omega_1) E_{inc}^{(v)}(\boldsymbol{r}, \omega_1)\right] = A_{e_{\omega_1}}\left[B_{\omega_1}\left[\overline{\chi}(\boldsymbol{r})\right] E_{inc}^{(v)}(\boldsymbol{r}, \omega_1)\right] \\
E_{scat}^{(v)}(\boldsymbol{r}, \omega_2) = A_{e_{\omega_2}}\left[\chi(\boldsymbol{r}, \omega_2) E_{inc}^{(v)}(\boldsymbol{r}, \omega_2)\right] = A_{e_{\omega_2}}\left[B_{\omega_2}\left[\overline{\chi}(\boldsymbol{r})\right] E_{inc}^{(v)}(\boldsymbol{r}, \omega_2)\right] \quad v = 1, \ldots, N_v, \quad \boldsymbol{r} \in \Omega \\
\cdots \qquad \cdots \qquad \cdots \qquad \cdots \\
E_{scat}^{(v)}(\boldsymbol{r}, \overline{\omega}) = A_{e_{\overline{\omega}}}\left[\chi(\boldsymbol{r}, \overline{\omega}) E_{inc}^{(v)}(\boldsymbol{r}, \overline{\omega})\right] = A_{e_{\overline{\omega}}}\left[\left[\overline{\chi}(\boldsymbol{r})\right] E_{inc}^{(v)}(\boldsymbol{r}, \overline{\omega})\right]
\end{cases} \quad (8)$$

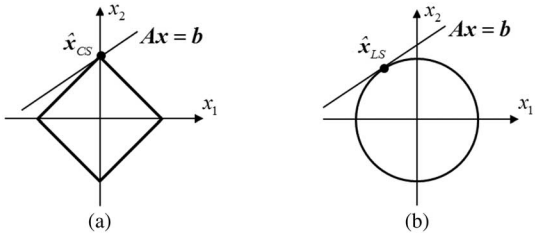

Fig. 2. Minimization of (a) L^1-norm and (b) L^2-norm problems.

stable. The basic idea of regularization is to replace the original ill-posed problem with a "nearby" well-posed problem whose solution approximates well the required one. Among all the various regularization techniques, the well-known Tikhonov regularization can be adopted. It consists in a quadratic penalty added to the objective function

$$\hat{\mathbf{x}}_{Tik} = \arg\min_{\mathbf{x}}\{\|\mathbf{A}\mathbf{x} - \mathbf{b}\|_{L^2}^2 + \gamma\|\mathbf{x}\|_{L^2}^2\} \qquad (13)$$

where the matrix $\mathbf{A}$ represents the forward model of the considered problem, and $\mathbf{b}$ the measured data. The previous regularization procedure establishes a restriction on the kind of the solution by enforcing its energy to be the lowest one. The regularization parameter $\gamma > 0$ provides a tradeoff between fidelity to the measurements and noise sensitivity. The previous functional can be properly minimized even if the number of data is lower than or equal to the number of unknowns, while in under-determined linear systems (i.e., $m << N$) without any kind of regularization, it is impossible to recover the unknown signal without any further information.

The use of standard regularization strategies, such as the Tikhonov one, which belongs to the class of the energy-constrained techniques, results in a very smooth reconstruction with poor spatial resolution. In this framework, if the additional assumption of sparse signal is assumed, then a L^1-norm regularization technique can considerably help us in finding a stable solution to our problem. In this case, the functional to be minimized becomes

$$\hat{\mathbf{x}}_{CS} = \arg\min_{\mathbf{x}}\{\|\mathbf{A}\mathbf{x} - \mathbf{b}\|_{L^2}^2 + \gamma\|\mathbf{x}\|_{L^1}\}. \qquad (14)$$

In the previous equation, the presence of the L^1-term forces the solution to be the sparsest one, according to the regularization parameter γ. Another advantage of L^1 regularization is linked to its feature of being less sensitive to the presence of outliers. The intuitive reason for which CS is able to recover sparse signals better than L^2-norm minimization is shown in Fig. 2 by using simply a 2-D example. In this figure, both L^1 and L^2 balls are depicted and given the linear problem we are dealing with, the solution to such an inverse problem may be found, from a graphical point of view, by gradually expanding the ball until it bumps with the line, which represents the set of all the $\mathbf{x}$ that have the same measurements. The first point of intersection is by definition the vector that solves the minimization procedure. It can be easily noted that one obtains the sparsest solution to the considered problem if the line does not intersect the ball in more than one point (for more detail, see [32] and [33]).

According to the previous information, in this paper, we propose a CS approach based on the class of iterative shrinkage-thresholding algorithms (ISTA) for solving problem (14), in which for each iteration a matrix–vector multiplication involving the model matrix and its transpose is used, and it is followed by a shrinkage/soft-threshold step [34]. More in detail, the general step of ISTA is

$$\boldsymbol{x}_{k+1} = \boldsymbol{T}_{\gamma t}\left(\boldsymbol{x}_k - 2t\boldsymbol{A}^{\dagger}\left(\boldsymbol{A}\boldsymbol{x}_k - \boldsymbol{b}\right)\right) \qquad (15)$$

where "t" is an appropriate stepsize, "$\boldsymbol{T}_{\gamma t}$" is the shrinkage operator, and "†" represents the transpose operation. In the optimization literature, this algorithm belongs to the gradient-based method and goes back till proximal forward–backward iterative scheme introduced in [35]. For such an algorithm, there is a widespread literature for the theoretical evaluation of the convergence rate that will not be dealt with in this paper (for more information, see [36] and [37]).

Therefore, if the hypotheses of CS hold true, then such a theory can be applied as an interesting alternative to classic regularization methods, most of which are based on quadratic terms (e.g., Tikhonov), entropy-type, or penalty functions, in order to improve reconstruction capabilities. In the framework of the linearized models, it is possible to apply the theory of CS that, according to the notation and symbols employed previously, drives in assuming $\boldsymbol{A} = \boldsymbol{L}^{MF}$, $\boldsymbol{b} = \boldsymbol{e}_{scatt}^{MF}$, and $\boldsymbol{x} = \overline{\boldsymbol{\chi}}_{2N_{cells}}$.

V. A CS-based Approach for Microwave Imaging: Performance Evaluation

After a quick review of some basics of CS theory, we are going to realize a numerical analysis of the performance of the proposed approach. As a first set of tests, let us consider the ideal situation of a free space environment, where the background is a homogeneous lossless medium with the imaging domain and targets located inside it. According to the preliminary results proposed in [38], in which a first coarse analysis of the robustness of the algorithm versus the noise has been proposed, we decided to choose as reference SNR the value of 20 dB for the noisy simulated data proposed in the following examples (the noise employed is an additive zero-mean white Gaussian one). Moreover, all the data have been generated by using a full-wave forward scattering model using a grid that is different from the one used to recover the contrast functions, in order to generalize the considered problem and avoid any kind of "inverse crime" [8].

Let us consider a first example at the operating single-frequency of 300 MHz, and consider a homogeneous, lossless background whose relative dielectric permittivity is equal to 1. The imaging domain is a square of size equal to $2\lambda \times 2\lambda$ in which three square scatterers whose side is $\lambda/5$ are located, and λ is equal to the wavelength in the background medium. Such scatterers have relative permittivities which belong to (1.1–1.2) and conductivities which belong to (0.8,1) mS/m (see Fig. 3). According to [39], the number of degrees of freedom for this example is about $(2\beta a + 1)^2/2 \approx 180$, which represents the maximum amount of independent data for this kind of configuration, with $\beta = 2\pi/\lambda$ representing the wavenumber in the

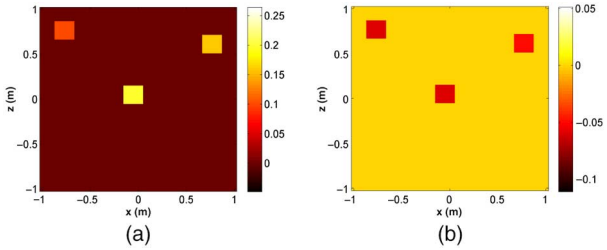

Fig. 3. Reference geometry for data reduction. (a) Real and (b) imaginary parts of contrast function.

homogeneous medium and a the radius of the smallest circle which completely includes the scatterers.

What we are going to show in this section is an evaluation of the potential performance of CS, since one can use such a theory to move toward two main directions: the first one wants to reduce the number of data but keeping good reconstruction capabilities compared with standard approaches, whereas the second one drives in gaining super-resolution, but without decreasing the number of data. Therefore, there is a kind of tradeoff between these two options.

In Figs. 4 and 5, a comparison between our approach and standard Tikhonov regularization procedure as function of the number of data is presented. In Fig. 4, we employed a number of data that is higher than the degrees of freedom for the considered geometry, and in this case, both CS and the standard Tikhonov regularization procedure manage to retrieve at least the support of the unknown objects; moreover, CS manages to retrieve in a quantitative way the values of the contrast profile quite well, whereas Tikhonov cannot manage such an issue. Looking at the numerical results depicted in Fig. 5, one can easily see that CS is still able to recover the unknown profile without losing so many details, even though we are dealing with a number of data that are much lower than the one established by the degrees of freedom. By having a look at Table I, one can see that even though the Tikhonov case seems to be also stable while reducing the number of data, it results that, from a quantitative point of view, CS is still working better than standard L^2-norm regularization. About Tikhonov regularization, all the examples considered in this work have been achieved by using a regularization parameter that has been chosen by means of a L-curve procedure.

The normalized reconstruction error is defined as

$$err = \frac{\|\tilde{\chi} - \chi_{true}\|_{L^2}^2}{\|\chi_{true}\|_{L^2}^2}. \tag{16}$$

All the errors of the previous and following examples are listed in Table I.

As it has been said before, another possible application of a CS-based approach is related to gain super-resolution in targets recovery. Let us consider a second example again using a single-frequency approach in which two square scatterers, whose size is equal to $\lambda/5$, are located inside the same imaging domain described in the previous example at an initial distance equal to $\lambda/2$, as shown in Fig. 6. Such a distance between the two scatterers is gradually decreased, till it reaches the value of $\lambda/10$. Reconstruction results are shown in Figs. 7 and 8.

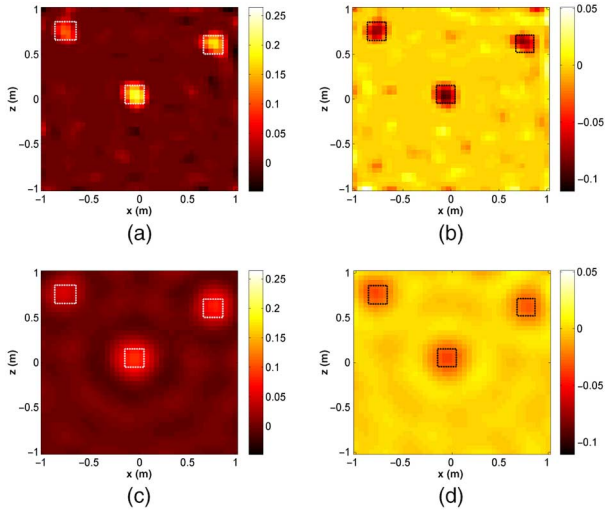

Fig. 4. Performance evaluation in a free space configuration: real and imaginary parts of reconstructed profile for both CS and standard Tikhonov regularization. Number of data: 14×14. (a) and (b) Proposed approach with CS ($err = 0.06$). (c) and (d) Tikhonov regularization ($err = 0.47$).

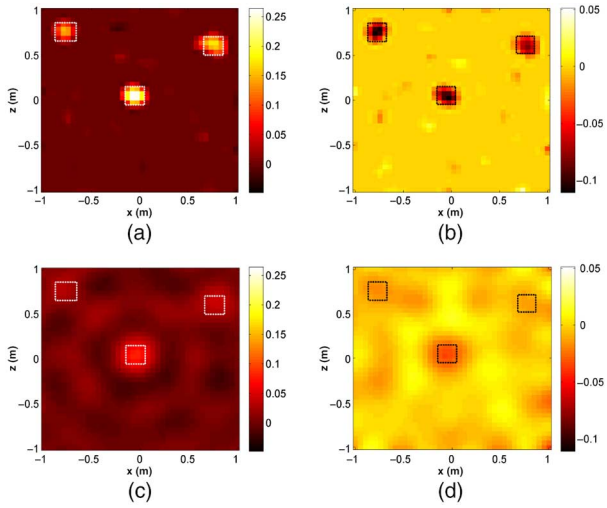

Fig. 5. Performance evaluation in a free space configuration: real and imaginary parts of reconstructed profile for both CS and standard Tikhonov regularization. Number of data: 8×8. (a) and (b) Proposed approach with CS ($err = 0.1$). (c) and (d) Tikhonov regularization ($err = 0.53$).

TABLE I
VALUES OF THE RECONSTRUCTION ERROR FOR THE EXAMPLES PROPOSED IN THE FREE SPACE CASE

	Data reduction $N_v \times N_m$		Super-resolution Distance between the two targets	
	14×14	8×8	$\lambda/2$	$\lambda/10$
Compressive sensing	0.06	0.1	0.12	0.23
Tikhonov regularization	0.47	0.53	0.41	0.46

Again, one can easily see that by using CS theory is possible to gain in terms of resolution by keeping fixed the number of involved data (which has been fixed at 14×14 for this example,

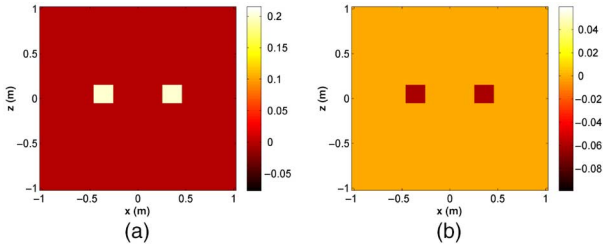

Fig. 6. Reference geometry for gaining super-resolution. (a) Real and imaginary (b) parts of contrast function.

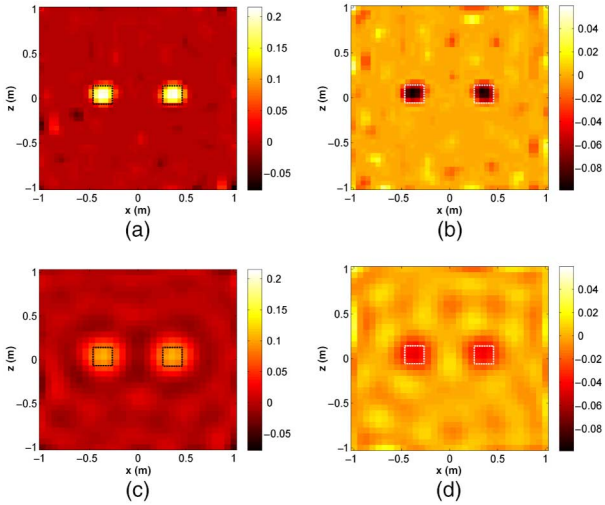

Fig. 7. Performance evaluation in a free space configuration: real and imaginary parts of reconstructed profile for both CS and standard Tikhonov regularization. Distance between the targets: $\lambda/2$. (a) and (b) Proposed approach with CS $(err = 0.12)$. (c) and (d) Tikhonov regularization $(err = 0.41)$.

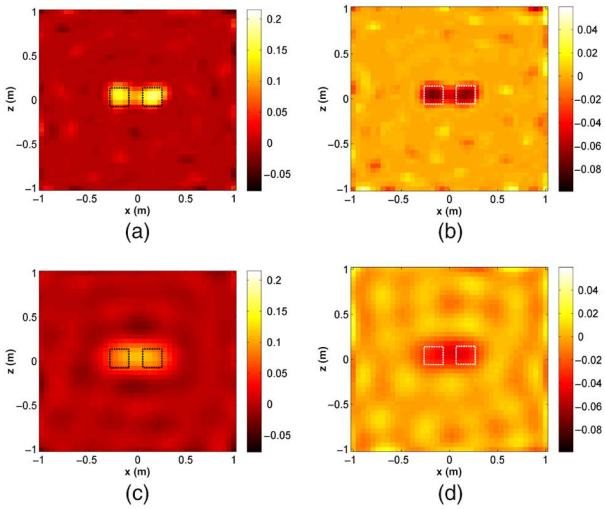

Fig. 8. Performance evaluation in a free space configuration: real and imaginary parts of reconstructed profile for both CS and standard Tikhonov regularization. Distance between the targets: $\lambda/10$. (a) and (b) Proposed approach with CS $(err = 0.23)$. (c) and (d) Tikhonov regularization $(err = 0.46)$.

since we have a multiview-multistatic configuration). Indeed, as conventional microwave imaging approaches suggest, standard resolution is about $\lambda/4$; conversely using CS, it is possible to go down till to a resolution of $\lambda/10$, preserving the capabilities

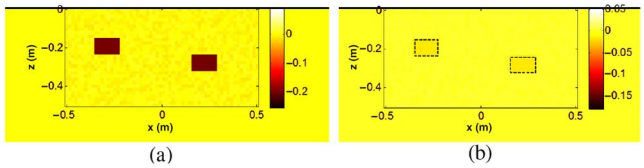

Fig. 9. Reference geometry for GPR applications. (a) Real and (b) imaginary parts of contrast function.

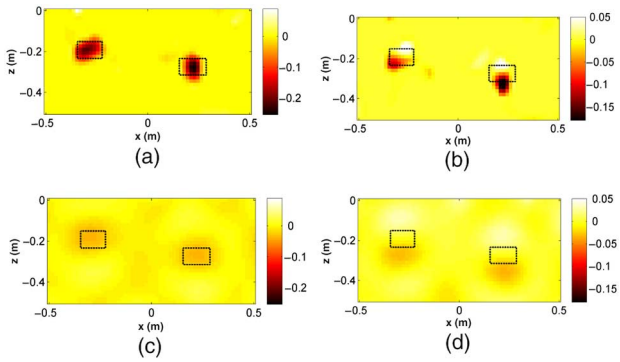

Fig. 10. Performance evaluation in an aspect-limited configuration: real and imaginary parts of reconstructed profile for both CS and standard Tikhonov regularization in the single-frequency case. (a) and (b) Proposed approach with CS $(err = 0.49)$. (c) and (d) Tikhonov regularization $(err = 0.96)$.

of the system to separate the two objects. Also for this example, reconstruction errors are reported in Table I.

VI. GPR Applications: Numerical Results

After the evaluation of the theoretical performance of the CS-based algorithm in the ideal free space environment, let us move on a more difficult case, which is the one proposed for GPR applications. Conversely to the previous analysis, in GPR applications, there is no longer a single homogeneous medium in which the targets are located, but the scenario is composed, again in an approximated fashion, by two homogeneous media that are separated by a planar interface, as shown in Fig. 9.

The first medium is air ($\epsilon_1 = 1$ and $\sigma_1 = 0$ S/m), whereas the second one represents a sandy lossless soil ($\epsilon_2 = 4$ and $\sigma_2 = 0$ S/m). The operating frequency is still 300 MHz and the imaging domain size is $2\lambda \times \lambda$, inside which two rectangular scatterers of size $\lambda/3 \times \lambda/6$ with permittivity equal to 3.2 and conductivity equal to $10^{-3}\,\mathrm{S/m}$ are buried. The line on which transmitters and receivers are located extends for a length equal to 4λ and consists of seven transmitters and seven receivers equally spaced and located in the same positions. As in the previous examples, in order to perform this numerical analysis, the data have been generated using a grid different from the one employed to realize the inversion, so to avoid any inverse crime. Moreover, the background medium has been corrupted by a 5% random inhomogeneity and also data for getting the results have been corrupted by 20-dB additive white Gaussian noise. In Fig. 10, some results are shown and a comparison with the standard Tikhonov regularization is proposed. Again, CS works better than the standard Tikhonov regularization, as confirmed by looking at the reconstruction errors. It is interesting

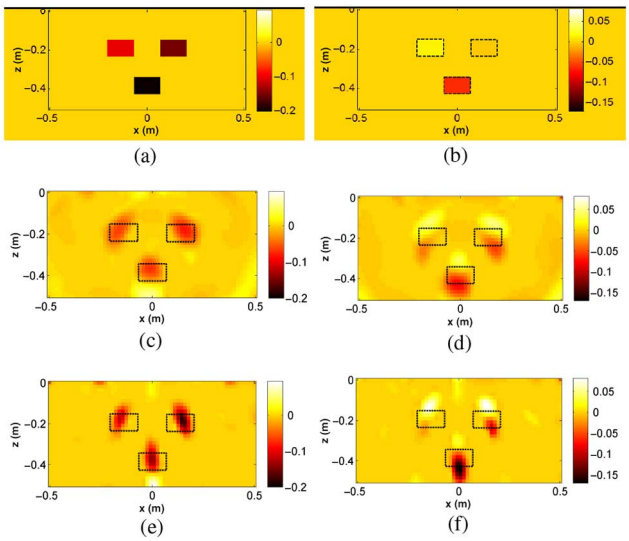

Fig. 11. Comparison between single-frequency and multifrequency approaches. (a) and (b) Reference profile, real and imaginary parts. (c) and (d) Proposed approach with CS (real and imaginary parts)—single-frequency ($err = 0.72$). (e) and (f) Proposed approach with CS (real and imaginary parts)—multifrequency ($err = 0.64$).

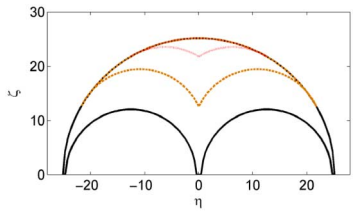

Fig. 12. Extension of the spectral coverage of the external operator as a function of the length of the measuring line. Red dotted line: short measurement line (λ). Brown dashed line: medium measurement line ($4 \times \lambda$). Black line: long measurement line ($10 \times \lambda$).

to note that in case of GPR applications, compared to the previous analysis developed in the ideal free space scenario, here the imaginary part of the reconstructed contrast profile differs from the reference one, since it mainly consists of two spots, which are located along the edges of the targets: such a behavior is due to the filtering properties of the external operator when considering the z-direction, i.e., the depth direction, that is the reason for observing this pattern [40]. As it can be easily seen, also in this example, Tikhonov regularization fails.

Let us show how it is possible to improve reconstruction capabilities, but in order to reach such an aim it is mandatory to add more independent information, and one can manage in such an issue by means of a multifrequency approach. As it has been said before, we employed a multifrequency CS-based approach to overcome the limitations due to a single-frequency method.

Let us consider the following example, in which the two media have the same electromagnetic features as those ones proposed in the previous subsurface reconstruction, but now the soil is a lossy one, with $\sigma = 1\,\mathrm{mS/m}$. Furthermore, the number of data employed in this example is equal to 25, since five transmitters and five receivers are used and data belong to the frequencies (100, 150, 200, 250, 300) MHz. The reference profile that we want to recover and the reconstructions obtained

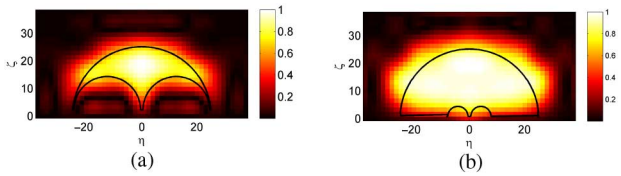

Fig. 13. Spectral coverage of the external operator: multiview-multistatic single-frequency (a) and multifrequency (b) configurations.

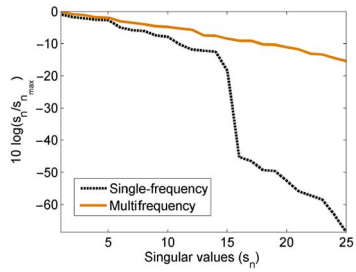

Fig. 14. Comparison between the singular values for the single-frequency and multifrequency approaches.

by using single-frequency and multifrequency approaches are sketched in Fig. 11. It is easy to note that the latter method works better than the former one. In order to understand why multifrequency works better than single-frequency, it is useful to think an example in which the background is lossless and the scatterers are buried at some wavelengthes in depth, since under these assumptions it is possible to evaluate analytically the relationship between data and unknowns (see [41]) that consists in a 2-D Fourier transform after using a nonlinear mapping for the Fourier variables (see [40]). Such a piece of information depends also on the length of the measuring line, which changes the spectral coverage of the external operator (see Fig. 12). More in details, the upper edge of the extension of the spectral coverage for the single-frequency case is represented by the red dotted line shown in Fig. 12, and the lower edge changes according to the length of measuring line. Moreover, the extension of the region in the Fourier domain, which represents the spectral coverage, varies according to the kind of considered configuration. As a matter of fact is depicted the spectral coverage for both the single-frequency and multifrequency multiview-multistatic cases for a measurement line of length 10λ in Fig. 13, supposed that both the previous hypotheses are valid. But since we are considering situations in which the targets are shallow enough and the kind of considered soil may be a lossy one, no analytical analysis can be proposed. Nevertheless, the numerical tool of the singular value decomposition (SVD) can help us to still prove the validity of the previous statements, even though the relationship between data and unknowns is no longer a Fourier transform. In Fig. 14, a comparison between the numerical SVD of the single and multifrequency cases is proposed. By looking at these figures, one can easily understand that for the multifrequency example, the number of singular values that are upon a certain threshold is greater than the one in the single-frequency case: such a behavior justifies the better reconstruction obtained using the multifrequency approach. However, the high values of the

reconstruction error are justified by the high error on the imaginary part of contrast function, and this is due to the nature of external operator.

VII. Conclusion

In this paper, a preliminary analysis of the performance of a CS-based approach for the detection and quantitative characterization of buried objects within the framework of a linear approximation has been proposed. In particular, an analysis of the performance of the CS-based algorithm in the canonical free space configuration has been discussed, in order to explore the two main strategies available to exploit the potentialities of such a theory. Moreover, these results have been compared with standard inversion procedures based on Tikhonov regularization and then improved by using a multifrequency approach. Due to the numerical tool of the SVD, the capabilities of the multifrequency and single-frequency approaches have been tested and compared in more complicated aspect-limited scenarios, confirming the improved qualities of the multifrequency reconstructions rather than the single-frequency ones by means of a numerical analysis of the spectral coverage of the external radiating operator.

Appendix

Let us start from (9), that is an operator equation which relates the data of the considered problem in the multifrequency framework with the unknowns at a fixed frequency (i.e., the maximum one in the selected bandwidth). In order to define explicitly the operator $\boldsymbol{L}^{MF}$, let us rewrite the equation mentioned before as

$$E^{(v)}_{scatt}(\boldsymbol{r}_m,\omega_f) = k_2^2 \iint_{\Omega} g_{21}(\boldsymbol{r}_m,\boldsymbol{r'},\omega_f)\cdot B_{\omega_f}\left[\overline{\chi}\left(\boldsymbol{r'}\right)\right] \cdot E^{(v)}_{inc}(\boldsymbol{r}_v,\boldsymbol{r'},\omega_f)\,d\boldsymbol{r'}, \quad \boldsymbol{r}_m,\boldsymbol{r}_v,\in\Gamma\,\forall m=1,\ldots,N_m \quad \forall v=1,\ldots,N_v, \quad \boldsymbol{r'}\in\Omega \tag{A1}$$

where $\boldsymbol{r}_m$ and $\boldsymbol{r}_v$ are the vectors defining the positions of receivers and transmitters, respectively, both supposed to belong to the same measurement line.

We can now discretize the imaging domain by using a grid of pixels whose size is small enough to let us assume that both the incident field and the contrast function can be considered constant inside each cell of the imaging domain [42], i.e., $E^{(v)}_{inc}(\boldsymbol{r}_v,\boldsymbol{r'},\omega_f) = E^{(v)}_{inc}(\boldsymbol{r}_v,\boldsymbol{r}_n,\omega_f)$, and $\overline{\chi}\left(\boldsymbol{r'}\right) = \overline{\chi}\left(\boldsymbol{r}_n\right)\forall\boldsymbol{r'}\in\Omega(\boldsymbol{r}_n)$, with $\boldsymbol{r}_n$ being the vector pointing at the center of the nth cell. With these assumptions, it is possible to write

$$E^{(v)}_{scatt}(\boldsymbol{r}_m,\omega_f) = k_2^2 \sum_{n=1}^{N_{cells}} \iint_{\Omega(\boldsymbol{r}_n)} g_{21}(\boldsymbol{r}_m,\boldsymbol{r'},\omega_f)\cdot B_{\omega_f}\left[\overline{\chi}(\boldsymbol{r}_n)\right] \cdot E^{(v)}_{inc}(\boldsymbol{r}_v,\boldsymbol{r}_n,\omega_f)\,d\boldsymbol{r'} = k_2^2 \sum_{n=1}^{N_{cells}} B_{\omega_f}\left[\overline{\chi}\left(\boldsymbol{r}_n\right)\right] \cdot E^{(v)}_{inc}(\boldsymbol{r}_v,\boldsymbol{r}_n,\omega_f)\cdot\left[\iint_{\Omega(\boldsymbol{r}_n)} g_{21}(\boldsymbol{r}_m,\boldsymbol{r'},\omega_f)\,d\boldsymbol{r'}\right]. \tag{A2}$$

Let us focus on the operator

$$B_{\omega_f}\left[\overline{\chi}\left(\boldsymbol{r}_n\right)\right] = \frac{1}{2}\left(1+\frac{\overline{\omega}}{\omega_f}\right)\cdot\overline{\chi}\left(\boldsymbol{r}_n\right) + \frac{1}{2}\left(1-\frac{\overline{\omega}}{\omega_f}\right)\cdot\overline{\chi}^{*}\left(\boldsymbol{r}_n\right) \tag{A3}$$

the issue consists in rewriting (A3) to express the operator $B_{\omega_f}[\cdot]$ as a function of the real and imaginary parts of the reference contrast function $\overline{\chi}$, i.e., $B_{\omega_f}\left[\overline{\chi}\left(\boldsymbol{r}_n\right)\right] = B_{\omega_f}\left[\overline{\chi}_{Re}\left(\boldsymbol{r}_n\right),\overline{\chi}_{Im}\left(\boldsymbol{r}_n\right)\right]$. To reach this aim, let us start from the equation which defines the contrast function at the selected reference frequency

$$\overline{\chi}\left(\boldsymbol{r}_n\right) = \frac{\overline{\epsilon}_{eq}\left(\boldsymbol{r}_n\right)}{\overline{\epsilon}_2\left(\boldsymbol{r}_n\right)} - 1 = \frac{\epsilon'_x\left(\boldsymbol{r}_n\right) - j\frac{\sigma_x(\boldsymbol{r}_n)}{\overline{\omega}\epsilon_0}}{\epsilon'_2\left(\boldsymbol{r}_n\right) - j\frac{\sigma_2(\boldsymbol{r}_n)}{\overline{\omega}\epsilon_0}} - 1 \tag{A4}$$

from equation (A4) and omitting the dependence on $\boldsymbol{r}_n$ to simplify the notation, one can easily find that

$$B_{\omega_f}\left[\overline{\chi}\right] = \frac{Re\left[\left(\overline{\chi}+1\right)\cdot\overline{\epsilon}_2\right] + j\cdot\frac{\overline{\omega}}{\omega_f}\cdot Im\left[\left(\overline{\chi}+1\right)\cdot\overline{\epsilon}_2\right]}{Re\left[\overline{\epsilon}_2\right] + j\cdot\frac{\overline{\omega}}{\omega_f}\cdot Im\left[\overline{\epsilon}_2\right]} - 1 \tag{A5}$$

and after a few manipulations, observing that $\overline{\chi} = Re\left[\overline{\chi}\right] + j\cdot Im\left[\overline{\chi}\right] = \overline{\chi}_{Re} + j\cdot\overline{\chi}_{Im}$ and $\overline{\epsilon}_2 = Re\left[\overline{\epsilon}_2\right] + j\cdot Im\left[\overline{\epsilon}_2\right] = \overline{\epsilon}_{2,Re} + j\cdot\overline{\epsilon}_{2,Im}$, we have

$$\begin{aligned} B_{\omega_f}\left[\overline{\chi}\right] &= \overline{\chi}_{Re} + j\cdot\frac{\overline{\omega}}{\omega_f}\cdot\frac{\overline{\epsilon}_{2,Re} + j\cdot\frac{\overline{\omega}}{\omega_f}\cdot\overline{\epsilon}_{2,Im}}{\overline{\epsilon}_{2,Re} + j\cdot\frac{\omega_f}{\overline{\omega}}\cdot\overline{\epsilon}_{2,Im}}\cdot\overline{\chi}_{Im} \\ &= \overline{\chi}_{Re} + j\cdot\alpha\cdot\overline{\chi}_{Im} \end{aligned} \tag{A6}$$

which relates the unknown profile at the reference frequency $\overline{\omega}$ to the generic frequency ω_f in the selected bandwidth. Therefore, in order to write the operator $\boldsymbol{L}^{MF}$ in (11) properly, one can handle real and imaginary parts of contrast profile at reference frequency separately, and this results in doubling the number of columns in the discrete version of such an operator.

References

[1] R. Persico and F. Soldovieri, "A microwave tomography approach for a differential configuration in GPR prospecting," *IEEE Trans. Antennas Propag.*, vol. 54, no. 11, pp. 3541–3548, Nov. 2006.

[2] R. Jamal, T. Olivier, D. Nicolas, and V. Serge, "Non-destructive microwave characterization and imaging of dielectric materials using a near field technique," in *Proc. 13th Mediterr. Microw. Symp.*, 2013, pp. 1–4.

[3] E. C. Fear, P. M. Meaney, and M. A. Stuchly, "Microwaves for breast cancer detection?," *IEEE Potentials*, vol. 22, no. 1, pp. 12–18, Feb. 2003.

[4] M. Sato, K. Takahashi, and J. Fujiwara, "Development of the hand held dual sensor ALIS and its evaluation," in *Proc. 4th Int. Workshop Adv. Ground Penetrat. Radar*, 2007, pp. 3–7.

[5] D. J. Daniels, "Surface-penetrating radar," *IEEE Electron. Commun. Eng. J.*, vol. 8, no. 4, pp. 165–182, Aug. 1996.

[6] J. M. Lopez-Sanchez and J. Fortuny-Guash, "3-D radar imaging using range migration techniques," *IEEE Trans. Geosci. Remote Sens.*, vol. 48, no. 5, pp. 728–737, May 2000.

[7] R. Scapaticci, G. Bellizzi, I. Catapano, L. Crocco, and O. M. Bucci, "An effective procedure for MNP-enhanced breast cancer microwave imaging," *IEEE Trans. Biomed. Eng.*, vol. 61, no. 4, pp. 1071–1079, Apr. 2014.

[8] D. Colton and R. Krees, Inverse Acoustic and Electromagnetic Scattering Theory, in Applied Mathematical Sciences, vol. 93. New York, NY, USA: Springer, 1992.

[9] F. Soldovieri, O. Lopera, and S. Lambot, "Combination of advanced inversion techniques for an accurate target localization via GPR for demining applications," *IEEE Trans. Geosci. Remote Sens.*, vol. 49, no. 1, pp. 451–461, Jan. 2011.
[10] Q. Zhu and L. M. Collins, "Application of feature extraction methods for landmine detection using the Wichmann/Niitek ground-penetrating radar," *IEEE Trans. Geosci. Remote Sens.*, vol. 43, no. 1, pp. 81–85, Jan. 2005.
[11] S. Delbo, P. Gamba, and D. Roccato, "A fuzzy shell clustering approach to recognize hyperbolic signatures in subsurface radar images," *IEEE Trans. Geosci. Remote Sens.*, vol. 38, no. 3, pp. 1447–1451, May 2000.
[12] P. D. Gader, J. M. Keller, and B. Nelson, "Recognition technology for the detection of buried landmines," *IEEE Trans. Fuzzy Syst.*, vol. 9, no. 1, pp. 31–43, Feb. 2001.
[13] N. Milisavljevic, "Analysis and fusion using belief functions theory of multisensor data for close-range humanitarian mine detection", Ph.D. dissertation, Ecole Nat. Superieure Telecommun., Paris, France, 2001.
[14] B. Scheers, M. Acheroy, and A. Vander Vorst, "Migration technique based on the time-domain model of the ground penetrating radar," in *Proc. SPIE Surf. Subsurf. Sens. Technol. Appl. III*, San Diego, CA, USA, 2001, pp. 111–119.
[15] J. Van Der Kruk, C. P. A. Wapenaar, J. T. Fokkema, and P. M. Van Den Berg, "Three-dimensional imaging of multicomponent ground-penetrating radar data," *Geophysics*, vol. 68, no. 4, pp. 1241–1254, Jul. 2003.
[16] L. Crocco, M. D'Urso, and T. Isernia, "New tools and series for forward and inverse scattering problems in lossy media," *IEEE Geosci. Remote Sens. Lett.*, vol. 1, no. 4, pp. 327–331, Oct. 2004.
[17] L. Lo Monte, F. Soldovieri, D. Erricolo, and M. C. Wicks, "Imaging below irregular terrain using RF tomography," *IEEE Trans. Geosci. Remote Sens.*, vol. 50, no. 9, pp. 3364–3373, Sep. 2012.
[18] I. Catapano, L. Crocco, R. Persico, M. Pieraccini, and F. Soldovieri, "Linear and nonlinear microwave tomography approaches for subsurface prospecting: validation on real data," *IEEE Antennas Wireless Propag. Lett.*, vol. 5, no. 1, pp. 49–53, Dec. 2006.
[19] R. Pierri, A. Brancaccio, and F. De Blasio, "Multifrequency dielectric profile inversion for a cylindrically stratified medium," *IEEE Trans. Geosci. Remote Sens.*, vol. 38, no. 4, pp. 1716–1724, Jul. 2000.
[20] L. Lo Monte, D. Erricolo, F. Soldovieri, and M. C. Wicks, "Radio frequency tomography for tunnel detection," *IEEE Trans. Geosci. Remote Sens.*, vol. 48, no. 3, pp. 1128–1137, Mar. 2010.
[21] L. T. Isernia, V. Pascazio, and R. Pierri, "A nonlinear estimation method in tomographic imaging," *IEEE Trans. Geosci. Remote Sens.*, vol. 35, no. 4, pp. 910–923, Jul. 1997.
[22] O. M. Bucci, L. Crocco, T. Isernia, and V. Pascazio, "Subsurface inverse scattering problems: quantifying, qualifying and achieving the available information," *IEEE Trans. Geosci. Remote Sens.*, vol. 39, no. 11, pp. 2527–2538, Nov. 2001.
[23] P. Meincke, "Linear GPR inversion for lossy soil and a planar air-soil interface," *IEEE Trans. Geosci. Remote Sens.*, vol. 39, no. 12, pp. 2713–2721, Dec. 2001.
[24] F. Soldovieri and R. Solimene, "Through-wall imaging via a linear inverse scattering algorithm," *IEEE Geosci. Remote Sens. Lett.*, vol. 4, no. 4, pp. 513–517, Oct. 2007.
[25] A. Liseno, F. Tartaglione, and F. Soldovieri, "Shape reconstruction of 2-D buried objects under a kirchhoff approximation," *IEEE Geosci. Remote Sens. Lett.*, vol. 1, no. 2, pp. 118–121, Apr. 2004.
[26] M. Bertero and P. Boccacci, Eds., *Introduction to Inverse Problems in Imaging*, 2nd ed., Bristol, U.K.: IOP Publishing Ltd, 1998.
[27] W. C. Chew, Ed., *Waves and Fields in Inhomogeneous Media*. Piscataway, NJ, USA: IEEE Press, 1995.
[28] I. Catapano, L. Crocco, and T. Isernia, "A simple two-dimensional inversion technique for imaging homogeneous targets in stratified media," *Radio Sci.*, vol. 39, pp. 1–14, 2004.
[29] T. Isernia, V. Pascazio, and R. Pierri, "On the local minima in a tomographic imaging technique," *IEEE Trans. Geosci. Remote Sens.*, vol. 39, no. 7, pp. 1596–1606, Jul. 2001.
[30] R. Autieri, G. Ferraiuolo, and V. Pascazio, "Bayesian regularization in non-linear imaging: Reconstructionfrom experimental data in microwave tomography," *IEEE Trans. Geosci. Remote Sens.*, vol. 49, no. 2, pp. 801–813, Sep. 2010.
[31] R. Autieri, M. DUrso, T. Isernia, and V. Pascazio, "Inverse profiling via an effective linearized scattering model and mrf regularization," *IEEE Geosci. Remote Sens. Lett.*, vol. 8, no. 6, pp. 1021–1025, Nov. 2011.
[32] E. J. Candes, J. Romberg, and T. Tao, "Stable signal recovery from incomplete and inaccurate measurements," *Commun. Pure Appl. Math.*, vol. 59, pp. 1207–1223, 2006.
[33] J. Romberg, "Imaging via compressive sampling," *IEEE Signal Process. Mag.*, vol. 25, no. 2, pp. 14–20, Mar. 2008.
[34] M. A. T. Figueiredo and R. D. Nowak, "An EM algorithm for wavelet-based image restoration," *IEEE Trans. Image Process.*, vol. 12, no. 8, pp. 906–916, Aug. 2003.
[35] G. B. Passty, "Ergodic convergence to a zero of the sum of monotone operators in hilbert space," *J. Math. Anal. Appl.*, vol. 72, no. 2, pp. 383–390, Dec. 1979.
[36] A. Chambolle, R. A. DeVore, N. Y. Lee, and B. J. Lucier, "Nonlinear wavelet image processing: Variational problems, compression, and noise removal through wavelet shrinkage," *IEEE Trans. Image Process.*, vol. 7, no. 3, pp. 319–335, Mar. 1998.
[37] I. Daubechies, M. Defrise, and C. D. Mol, "An iterative thresholding algorithm for linear inverse problems with a sparsity constraint," *Commun. Pure Appl. Math.*, vol. 57, no. 11, pp. 1413–1457, Nov. 2004.
[38] M. Ambrosanio and V. Pascazio, "A compressive sensing based approach for microwave tomopraghy and GPR applications," in *Proc. IEEE Int. Geosci. Remote Sens. Symp.*, 2014, pp. 3144–3147.
[39] O. M. Bucci and G. Franceschetti, "On the degree of freedom of scattered fields," *IEEE Trans. Antennas Propag.*, vol. 37, no. 7, pp. 918–926, Jul. 1989.
[40] R. Persico, R. Bernini, and F. Soldovieri, "The role of the measurement configuration in inverse scattering from buried objects under the distorted Born approximation," *IEEE Trans. Antennas Propag.*, vol. 53, no. 6, pp. 1875–1887, Jun. 2005.
[41] G. Leone and F. Soldovieri, "Analysis of the Distorted Born Approximation for subsurface reconstruction: Truncation and uncertainties effects," *IEEE Trans. Geosci. Remote Sens.*, vol. 41, no. 1, pp. 66–74, Jan. 2003.
[42] J. Richmond, "Scattering by a dielectric cylinder of arbitrary cross section shape," *IEEE Trans. Antennas Propag.*, vol. 13, no. 3, pp. 334–341, May 1965.

Michele Ambrosanio (S'13) was born in Naples, Italy, in 1987. He received the B.S. and M.S. degrees (*summa cum laude*) in biomedical engineering from the University of Naples "Federico II," Napoli, Italy, in 2009 and 2012, respectively. He is currently pursuing the Ph.D. degree in information engineering at the University of Naples "Parthenope," Napoli, Italy.

His research interests include electromagnetic inverse scattering problems for noninvasive diagnostics, ground penetrating radar, compressive sensing, numerical methods for forward scattering problems, and biomedical applications of microwave imaging.

Vito Pascazio (SM'11) received the "Laurea" degree (*summa laude*) in electronic engineering from the Universit di Bari, Bari, Italy, in 1986, and the Ph.D. degree in electronic engineering and computer science from the Universit di Napoli Federico II, Napoli, Italy, in 1990.

In 1990, he was at the Research Institute on Electromagnetics and Electronic Devices (IRECE), Italian National Council of Research (CNR), Napoli, Italy. Currently, he is a Full Professor and Chair of the Department of Engineering, Universit di Napoli Parthenope, Napoli, Italy. From 1994 to 1995, he was a Visiting Scientist at the Laboratoire des Signaux et Systemes of the Ecole Superieure dElectricite (Supelec), Gif sur Yvette, France, and from 1998 to 1999, with the Universite de Nice Sophia-Antipolis, Nice, France. He is also Director of National Laboratory of Multi-Media Communications, Italian Consortium of Telecommunications (CNIT), Napoli, Italy. He has authored more than 170 technical papers. His research interests include remote sensing, linear and nonlinear estimation, with particular emphasis to image computing and processing, and reconstruction of microwave and radar images.

Dr. Pascazio is a General Co-Chairman of next IGARSS-2015 conference. He was the recipient of the Philip Morris Prize for Scientific and Technological Research, in 1990.